Kinematic Analysis of Human Gait Cycle and Squat

Alexandra Santos[1], Diogo Marques[1], Filipa Baltazar[1] and Rita Martins[1]

[1] *Instituto Superior Técnico, Integrated Master's in Biomedical Engineering,*
{alexandrabettencourt, diogo.m.marques, a.filipa.baltazar ,rita.r.martins.}@tecnico.ulisboa.pt

ABSTRACT — *Kinematic analysis can play major roles in biology, sports and medicine, making its understanding crucial in these fields. In the present work we performed a kinematic analysis of both the gait cycle and squat. For that, we modeled the human body as a multibody system and computed its position, velocity and acceleration analysis, by implementing a general-purpose program in MATLAB and using the data acquired in the Biomechanics of Motion Lab at Instituto Superior Técnico. The model was employed to analyse the gait cycle and squatting motion of a healthy female at the level of the lower limb joints (hip, knee and ankle) and muscles, leading to robust results, which allow for sufficient immediate analysis of the motions at hand as well as for the extrapolation of data for a more refined analysis.*

1 Introduction

Kinematics is the study of a given system's motion, specifically its position, velocity and acceleration, regardless of the forces involved in the said motion. Since the human body can be modeled as a multibody system (several rigid bodies connect by revolute joints in 2D), it's possible to compute its motion analysis. The main goal of the present work is to develop a general-purpose MATLAT program that allows the formulation and resolution of the motion's equations for each body part in two types of motion: the gait cycle and the squat.

1.1 Motivation

Human body movements require a highly coordinated mechanical interaction between bones, muscles, ligaments and joints, and play a major role in our day-to-day life. Kinematics is, for that, a very important tool in a variety of fields, and has applications such as therapy and diagnosis, optimization of athletic performances, or even the design of biomedical devices, such as prosthesis.

Since the gait cycle is one of the most common human movements, its analysis can be of high interest and can help treat difficulties in an individual's walking. On the other hand, the proper performance of the squat benefits not only athletes and their performance, but a grand majority of the population, since it is considered one of the best exercises to improve quality of life, due to its ability to recruit several muscle groups [1].

2 Description of Motion

2.1 Gait Cycle

The gait cycle is the most common of all human movements and consists of a repetitive pattern of steps and strides. To clarify the movement, the gait cycle is defined as the time interval between two successive occurrences of one of the repetitive events of walking. With this in mind, each step refers to all the events between consecutive heel strikes of both feet, while each stride corresponds to the whole gait cycle of one limb. The gait cycle can be divided

into two main phases, the stance phase, which refers to the entire period during which the foot is on the ground (60% of the gait cycle), and the swing phase, which refers to the time the foot is in the air for limb advancement (40% of the gait cycle) [2].

As seen in Figure 1(A), the stance phase begins with the initial contact of the reference foot with the ground (**heel strike**) and is followed by a loading response until the opposite foot leaves the ground. The opposite foot continues to progressively lift up to the air, until the **heel rise** until the center of mass is directly above the reference foot (**midstance)**. The foot then progressively returns to the ground and reaches it (**opposite initial contact**) at the end of the terminal stance. Lastly, the stance phase finishes with the **pre swing**, that is, the moment the reference foot's toes leave the ground (**toe off**).

Finally, the swing phase corresponds to the advancement of the reference limb and is divided into three subphases: **initial swing**, which goes from reference toe off to adjacent feet, **midswing**, which ends with the vertical tibial position, and **terminal swing**, which is a deceleration phase from vertical tibial position to next initial contact.

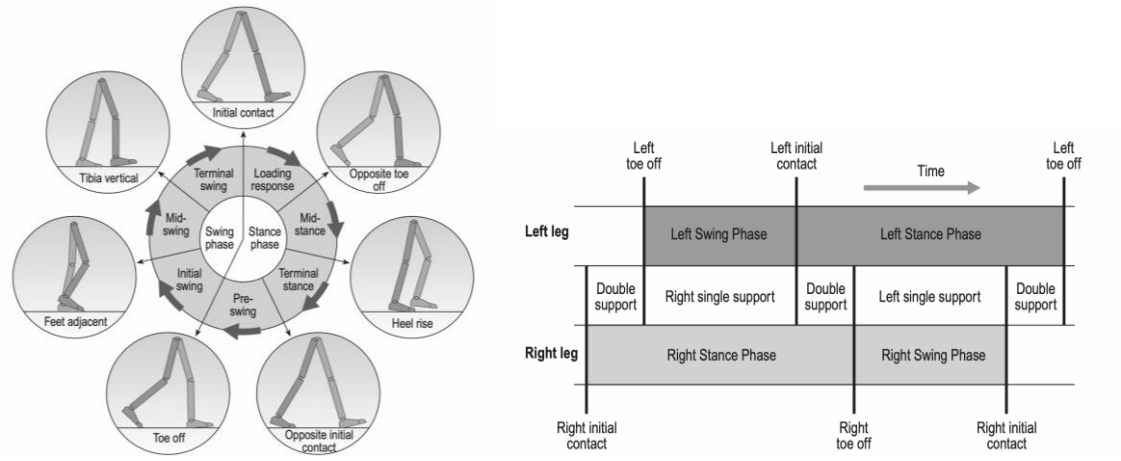

(A) (B)

Fig. 1: Gait cycle: (A) Positions of the legs during a single gait cycle by the right leg (darker gray); (B) Timing of single and double support during a little more than one gait cycle, starting with right initial contact [1].

2.2 Squat

Fig. 2: Squat motion.

The squat is a type of movement which measures lower body and trunk strength and requires coordinated actions of the torso and the major joints of the lower body, leading to injuries when performed incorrectly. The squat starts in upright position and proceeds with a descending of the body's center of mass until a desired squat depth (which is measured by the degree of flexion at the knee) is achieved, followed by ascension back to upright position [1]. It's important to note that, in order to avoid injuries, the feet should be at shoulder width, and the lowering should be performed without letting the knees surpass the toe tips or the heels leave the floor.

3 Methodology

In order to analyze the two motions described above, experimental observations were performed with the aid of markers and a specialized motion tracking system. The acquired data was then handled based on the theory of kinematics, meaning that the individual body sections were considered rigid bodies and the proper constraints were applied to the system.

3.1 Variables

Kinematic variables are involved in the motion's description and include linear and vertical displacements, velocities and accelerations. Regarding the displacements, the data is acquired from any anatomical landmarks: the center of gravity of body segments, the centers of rotation of joints or the extremes of the limb segments [3].

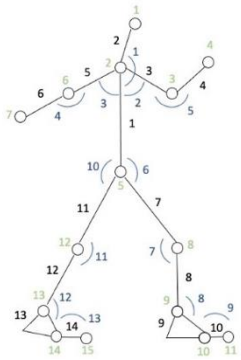

Fig. 3: Biomechanical model used for the analysis. While the 15 markers are identified with the green color, the 14 rigid bodies are identified with black, and the 13 revolute joints are identified with blue.

Although the data acquired in Biomechanics Laboratory was in a 3D setting, we chose to project it onto a 2D sagittal plane, in order to simplify and facilitate the implementation and analysis. **Figure 3** shows an illustrative scheme of the biomechanical model used. It is important to note that 17 markers were used in the laboratory, and the model chosen consists of only 15 markers, due to a simplification in the shoulders and hips, where only the midpoints were computed (marker 2 for the shoulders and 5 for the hips). Besides these two exceptional cases, both left and right heels were not considered, as only 2 markers are necessary to represent a linear rigid body such as the foot, and these would only add aesthetic value. Since each body consists of two markers, the model has a total of 14 rigid bodies, connected by 13 revolute joints.

3.2 Kinematic Analysis of a Multibody System

For the analysis of the multibody system represented in **Figure 3**, cartesian coordinates were used. Two types of frames will be considered: a fixed global coordinate system ($\boldsymbol{x}$,$\boldsymbol{z}$) and a local one ($\boldsymbol{\xi}$,$\boldsymbol{\eta}$), relative to each body. With that being said, each body is characterized by three coordinates relative to the center of mass: two translations in $\boldsymbol{x}$ and $\boldsymbol{z}$ (sagittal plane), and one rotation between the global axis $\boldsymbol{x}$ and the local axis ξ of the body [4][5]. The joints are defined by the relationship between the bodies they connect.

The normalized position for each body's center of mass was defined by its proximal or distal position along the segment, according to anthropometric data found in literature. The table with the data is present in **Appendix A**.

In order to perform the kinematic analysis, the first thing to do is establish the generalized coordinates vector, which consists of a column vector containing all the coordinates used to describe the system. This vector is

described in equation 1, where $\boldsymbol{r_i}$ is the position of the center of mass and $\boldsymbol{\theta_i}$ is the angle of each body i. Since our multibody system is composed of 14 bodies, each defined by 3 coordinates, we should expect a total of 42 (NBodies x NCoordinates) coordinates necessary to describe the system, yet, seeing as $\boldsymbol{r_i}$ is composed of 2 coordinates, the vector $\boldsymbol{q}$ will have 28 entries.

$$\boldsymbol{q} = \begin{bmatrix} \boldsymbol{r_i} \\ \boldsymbol{\theta_i} \end{bmatrix} \qquad \boldsymbol{r_i} = \begin{bmatrix} \boldsymbol{x_i} \\ \boldsymbol{z_i} \end{bmatrix} \tag{1}$$

The second step is to form the vector of kinematic constraints, which is also a column vector, where each component describes the constraints associated with each coordinate of the system. Our goal is to find the roots or solutions to the algebraic equations composing the vector, following **equation 2** [4].

$$\boldsymbol{\Phi(q,t)} = [\boldsymbol{\Phi_1} \quad \boldsymbol{\Phi_2} \quad \boldsymbol{\Phi_3} \cdots \boldsymbol{\Phi_{42}}]^{\boldsymbol{T}} = \mathbf{0} \tag{2}$$

The number of the system's degrees of freedom is given by **equation 3**, bearing in mind that a revolute joint allows only one translation, so in 2D it constraints 2 degrees of freedom (*dof*). Seeing as there are only 16 degrees of freedom, the other 26 equations in the constraint vector will describes the interdependency of the coordinates, which represent the restrictions introduced in the system by the joints and are therefore called revolute constraints, defined in equation 5.

$$\boldsymbol{Ncoord - Nrev.constraints = 3 \times 14 - 2 \times 13 = 42 - 26 = 16\ dof} \tag{3}$$

$$\boldsymbol{\Phi(\mathbf{q},\mathbf{t})^{(rev,2)} = r_i^P - r_j^P = (r_i^P + AS'^P_i) - (r_j + AS'^P_j)} \tag{4}$$

In **equation 4**, $\boldsymbol{i}$ and $\boldsymbol{j}$ represent the adjacent bodies, and P the center of the joint that connect the two bodies, which can be considered two different coincident points: $\boldsymbol{P_i}$ on body $\boldsymbol{i}$ and $\boldsymbol{P_j}$ on body $\boldsymbol{j}$. The local coordinates of P are given by $\boldsymbol{S'^P_{i,j} = [\xi_{i,j}, \eta_{i,j}]}$ and can be transformed into global coordinates using the rotation matrix $\boldsymbol{A}$ given by $\boldsymbol{\theta}$.

The driving constraints are additional constraint equations and represent each independent coordinate as a function of time [4]. To have a determined system, the number of drivers equals the number of degrees of freedom, 16, and, in this case, they can be of two types. The first type of drivers is defined by the angle of each of the 13 joints (the angle between the two bodies connected by each joint), so it involves 13 drivers. The second type, which encompasses 3 drivers, describes the absolute coordinates of the system, and are applied to the trunk (body 2 in **Figure 3**). The equations used for the two types of driver constraints are shown in **equations 5** and **6**, respectively.

$$\boldsymbol{\Phi(q,t)^{(drv,1)} = \theta_i - \theta_j - \theta_{ij}(t)} \tag{5}$$

$$\boldsymbol{\Phi(q,t)^{(drv,2)}} = \begin{bmatrix} \boldsymbol{r_i - r_i^0} \\ \boldsymbol{\theta_i - \theta_i^0} \end{bmatrix} \tag{6}$$

With $\boldsymbol{\theta_i}$ being the angle of body $\boldsymbol{i}$, $\boldsymbol{\theta_j}$ the angle of body j and $\boldsymbol{\theta_{ij}}$ the angle formed by the joint connecting bodies $\boldsymbol{i}$ and $\boldsymbol{j}$.

Having all the necessary variables and conditions, and since the system is non-linear, the next step is to conduct the position analysis with the Newton-Raphson method, described in **equation 7**.

$$\boldsymbol{\Phi(q,t) = 0} \Rightarrow \begin{cases} \boldsymbol{q_{i+1} = q_i - [\Phi_{qi}(q,t)]^{-1} \Phi_{qi}(q,t)} \\ \boldsymbol{|q_{i+1} - q_i| \leq \varepsilon} \end{cases} \tag{7}$$

With $\boldsymbol{q_i}$ being the initial estimate for position, $\boldsymbol{\varepsilon}$ the tolerance and $\boldsymbol{\Phi_{qi}}$ the Jacobian matrix of the constraint vector.

Finally, we proceed to analyze the velocity and acceleration, and for that we derive the position and velocity equations in order of time, obtaining equations 8 and 9, respectively [5].

$$\boldsymbol{v} = \dot{\boldsymbol{\Phi}}(\boldsymbol{q}, \boldsymbol{t}) = \boldsymbol{\Phi_q}\dot{\boldsymbol{q}} = -\frac{\boldsymbol{\partial \Phi}}{\boldsymbol{\partial t}} \tag{8}$$

$$\boldsymbol{\gamma} = \ddot{\boldsymbol{\Phi}}(\boldsymbol{q}, \dot{\boldsymbol{q}}, \boldsymbol{t}) = \boldsymbol{\Phi_q}\ddot{\boldsymbol{q}} = -\frac{\boldsymbol{\partial^2 \Phi}}{\boldsymbol{\partial t^2}} \tag{9}$$

3.3 Implementation

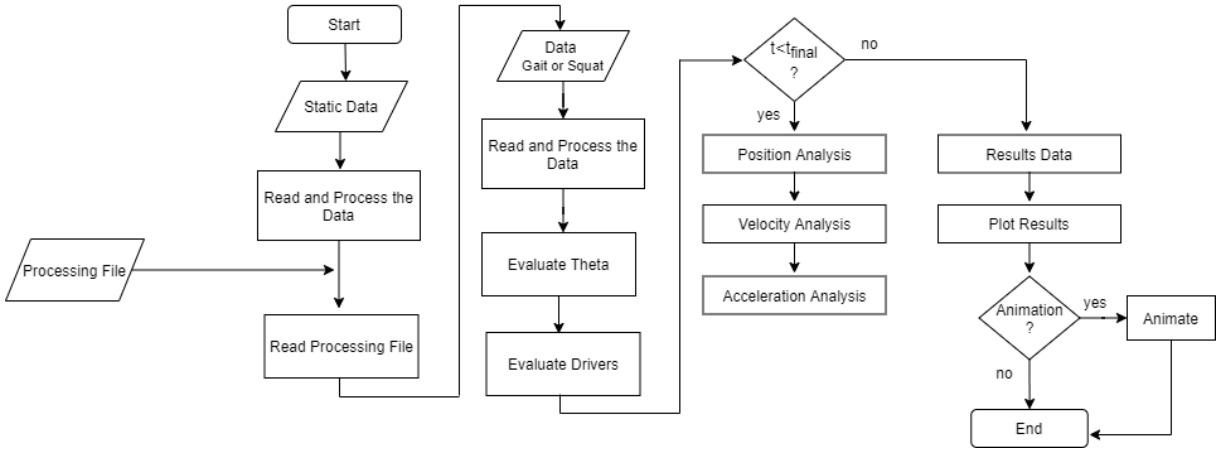

Fig. 4: Flowchart of the implemented kinematic analysis program

3.3.1 Pre-Processing

Before being able to use the coordinates registered at the laboratory for the different trials (i.e, for the static, gait and squat data), a pre-processing step had to be done.

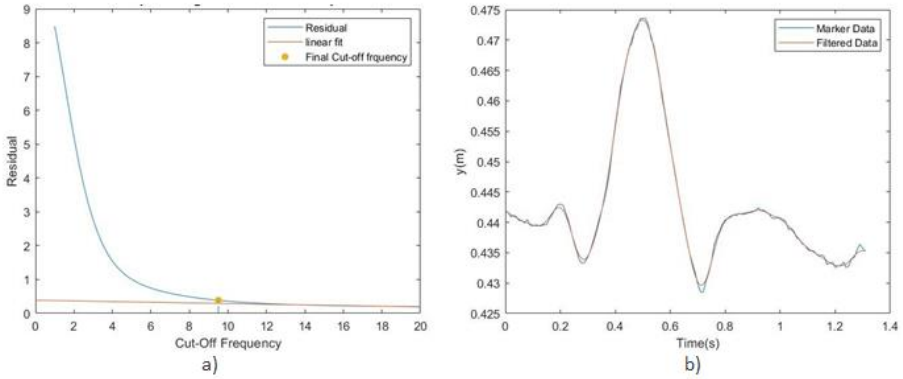

Fig. 5: Filtering of the coordinates. a) Residual plot over cut-off frequencies in a range from 1 to 20Hz (blue) and linear fit to the obtained residual data with 95% correlation (red). The chosen cut-off frequency (yellow point) is such that the residual is equal to the value at $y = 0$ of the linear fit ($y = ax + b$); b) Comparison between raw and filtered positions of the Left Knee marker.

The files received from the laboratory are **.tsv files**, which not only contain the three coordinates ($\boldsymbol{x}$,$\boldsymbol{y}$ and $\boldsymbol{z}$) for every time instant, but also specific information regarding the data that was acquired, such as the number of time frames, cameras and markers. Bearing this in mind, and since the analysis is only performed in the sagittal plane, the function "**ReadProcessData**" was implemented to select only the desired coordinates and filter them, as there

is inherent noise from the experiment. The filtration is performed by applying a low-pass Butterworth filter to each marker. The estimation of the cut-off frequency is done based on a linear regression with 95% of correlation to the residuals, which are calculated for cut-off frequencies ranging from 1 to 20Hz, as shown in **Figure 5 a)**.

3.3.2 Processing

Throughout our program, a set of global struct variables is defined, and its organization is shown in table 1, in **Appendix B**.

Before starting the analysis, itself, the information about the multibody system to be studied (bodies, joints and drivers, which contain the information for the driving constraints) was provided in a .txt file which is then read by the function "**ReadProcessingFile**". Having the information about the system, the data from the static acquisition allowed the computation of the average length of each body of our model.

Another necessary information for the kinematic analysis is the position of each joint delimiting a body relative to its center of mass in the reference frame of the body and the orientation of said body in the reference frame of the laboratory for each time frame. To obtain information for the drivers, cubic splines were applied to the now organized data, that is, either to the angle of two bodies sharing a joint or to the coordinate of a body, depending on the type of driver as described previously.

Once we have completed the definition of our global variables **Body** and **Jnt,** we were then able to compute the position (q), velocity (qd) and acceleration (qdd) of the center of mass and orientation of each body, based on the Newton-Rapson method, as mentioned in section 3.2. Once our analysis was finished, the most important variables of our program were also stored in a new variable, **Output**, for easier plotting and animating the results.

4 Results and Discussion

In this section, we will deal with analyzing and commenting the most relevant results obtained with our model. Further results can be found in the "Appendix" section of the report, but will often be alluded to, since they verify the solidity of the main results discussed in this section.

First and foremost, it is important to note that, for as good as measuring instruments and the model itself may be, there is always some inherent variability to the motion, which makes it so that separate, healthy individuals with similar characteristics may nonetheless exhibit slightly different motion patterns [2]. Therefore, it is more relevant to analyze the progression of the motion itself in each individual, rather than absolute values of, for instance, angles and velocities. In this way, we allow for the individual to serve as its own "control" and are better prepared to compare the trend in the subject's motion with the relevant patterns that are presented in literature.

Furthermore, it has been pointed out that there is no international consensus as to how to calculate the angles of the lower limb joints are defined and measured. In this work, we utilized the internal product of the two vectors (which represent the individual body parts) to calculate the joint angles, which can lead to different values for each stage of the movements, when compared to the literature. Nevertheless, the progression of the movement is the crucial factor here, and so we will be comparing the trend lines instead of the values of the angle.

The data that served as the basis for this study was obtained from a healthy 21-year-old white female.

4.1 Gait cycle

As previously shown, the gait cycle encompasses different phases, each with its own subdivisions. In this section, we will perform an analysis of some relevant parameters that were obtained by our model. It is crucial to see that these can be easily extrapolated to extract even more information, such as the step length, cadence, cycle time and speed, as well as the moments and powers of each joint. However, since the main goal of our work was to produce a functioning model, a more reductionist approach will be followed.

The gait cycle that was performed refers to the right limb.

4.1.1 Kinematic analysis

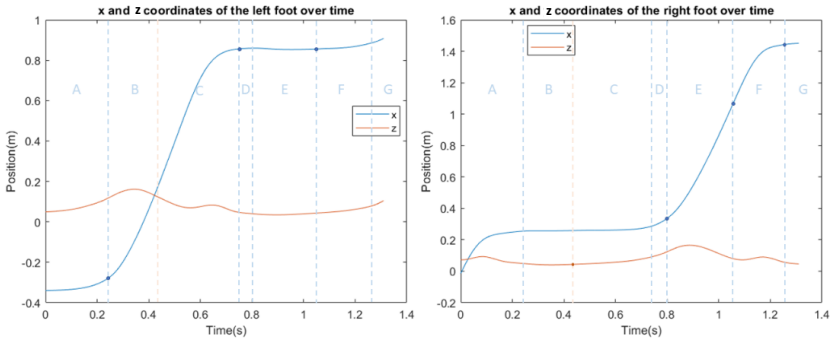

Figure 6: Different phases of the gait cycle as seen in our results. The dots indicate which coordinate of which foot was responsible for the initiation of the next phase of the cycle. A – Loading response; B – Mid-stance; C – Terminal stance; D – Pre-swing; E – Initial swing; F – Mid-swing; G – Terminal swing.

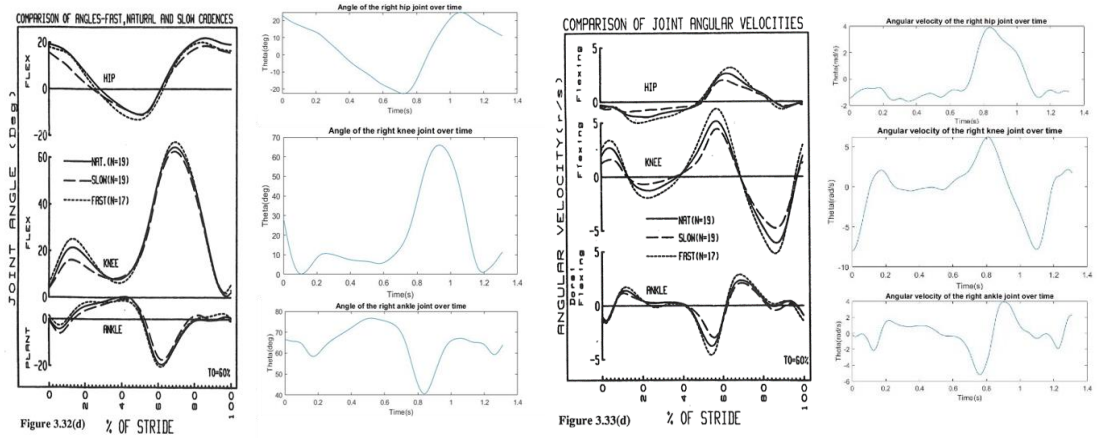

Figure 7: Comparison of results from the model with results from the literature [6] regarding angle and angular velocity of hip, knee, and ankle.

In a healthy individual, it is expected that the Stance phase takes up about 60% of the time of the gait cycle, while the Swing phase takes up the other 40% [2]. As shown in **Figure 6**, everything indicates that our subject follows this pattern, with 61.5% of the gait cycle being occupied by the Stance phase and the remaining 38.5% belonging to the Swing phase. We also obtained the value of approximately 108 steps per minute, which corresponds to the cadence [2]. The individual moments of the gait cycle are also depicted, and also appear to correspond to what was expected for a healthy individual, based on the current literature. No abnormalities were detected in what regards step length, with both limbs presenting similar behavior.

In addition to the different phases of the gait cycle, the angles of relevant joints (hip, knee, ankle) were also analyzed, as well as their angular velocity and acceleration. The extensive results of these analyses can be found in **Appendix C**. Indeed, in regard to the movement of the lower limbs and to the behavior of their joints, the subject appears to not have any traits of a pathological gait (**Figure 7)**, while showing a symmetry of motion between the right limb and left limb, albeit that said symmetry is delayed, due to the natural characteristics of the gait cycle.

These results strongly indict that our model is robust for the analysis of the gait cycle, as well as that our investigation subject does not have any anomalies in their gait.

4.1.2 Muscle activation

Muscle activation patterns were analyzed in major muscles of the lower limb, namely the Gastrocnemius Medialis, the Tibialis Anterior, the Rectus Femoris and the Biceps Femoris. These muscles are crucial for leg movements as pathologies associated with gait can often be traced back to malfunctions of the muscle groups. Once again, the results obtained in our work correspond to what was expected based on the literature, as can be seen in **Figure 8** and **Appendix E**.

Looking at the activation of the Tibialis anterior, for instance, we notice an early spike, followed by a dip and a prolonged absence of activity, until the muscle is activated once more, initially with a lower level of electric activity, but ending on yet another spike. Logically, this pattern is different for each muscle/muscle group, but we have found that our results resemble those obtained by previous authors.

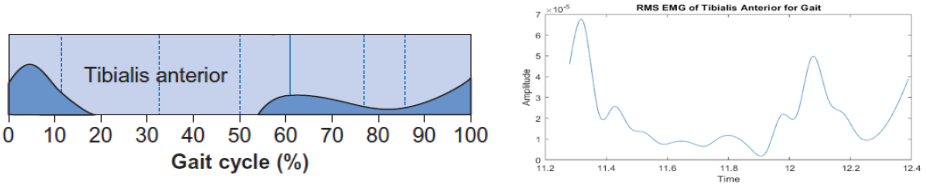

Figure 8: Activation pattern of the Tibialis Anterior during the gait cycle. Left - adapted from the literature [2]; Right - results obtained with our model.

4.2 Squat

Even though the model appears to be robust for the gait cycle, it must be valid for the analysis of any generic motion. Therefore, we analyzed a squatting motion (as described in section 2.2) of the same volunteer, which produced the results displayed in **Appendices F** and **H**. In this sequence of movements, the squatting motion was repeated 3 times, which originated a 3-way repetition of the same pattern across the board. Although unintentional, this phenomenon proved useful in validating the measurement instruments, both regarding to their function and the stability of their placement on the subject's body.

4.2.1 Kinematic analysis

As for the kinematic analysis of the movement, we can see that there is a nearly perfect symmetry in results with respect to the sagittal plane (**Appendix F**). Thus, the workload is distributed evenly between both lower limbs, which in turn hints at the fact that, since the subject does not favor one leg over the other, they are most likely healthy. The fact that the results obtained with our model are quite close to those that can be found in current literature [7] confirms that we have produced a robust model for kinematic analysis, since it was also verified that the subject was, indeed, healthy. The analysis of the squats themselves reveals us that the subject performed half-

squats, a movement in which the angle of the knee joint ranges from 70º to 100º. The angles, angular velocities and angular accelerations of each lower limb joint were also calculated, as seen in Appendices E.1 and E.3.
Since the squat is a voluntary and highly modifiable motion, its phases are hard to characterize meticulously. However, it is still possible to clearly distinguish the main phases of the movement, namely acceleration and deceleration, from the data obtained with the kinematic model (**Figure 9)**. In doing so, we see that the acceleration phase is slightly longer than the deceleration phase, which indicates a controlled descent and a rapid rise. This particular movement pattern can be useful to train lower limb muscles to support heavier loads, especially if the bodyweight of the athlete is incrementally supplemented with additional external weights. **Figure 10** shows that the results obtained with our model are mostly in accordance with the literature.
The data obtained in this section can also be extrapolated for further calculations, which depend on the ultimate goal of the movement. For an athlete it might be crucial to understand how to perfectly balance the movement and optimize the performance of its individual steps, while an orthopedic doctor might be more interested in the total amplitude of the patient's joints or the symmetry of the motion.

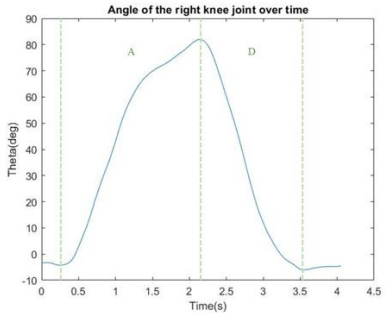

Figure 9 – Kinematic analysis of the angle of right knee joint during squat, with representation of both phases of the movement (A – Acceleration phase; D – Deceleration phase).

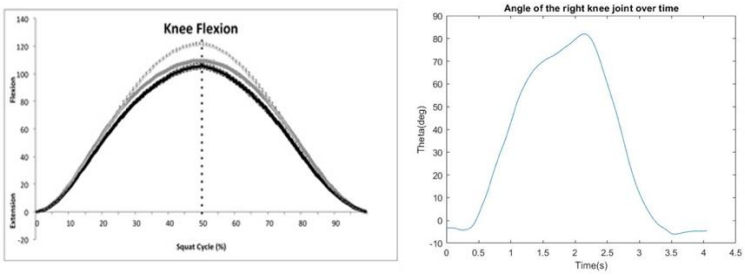

Figure 10: Comparison of results from the model with results from the literature [8] regarding the angle of the knee.

4.2.2 Muscle activation

Muscle activation was measured in the same muscle groups as seen for section 4.1.2, both due to convenience and to the fact that these are indeed the most relevant muscles for the squatting motion [8]. Indeed, Dionisio et al. characterized the activation patterns of various muscles, not only in pathological conditions, but in healthy conditions as well. The data obtained for healthy subjects closely resemble our own. If we look once more at the behavior pattern of the Tibialis Anterior (**Figure 11**), we can see that it is mostly inactive during the first half of each squat, spiking in activity for the latter part of the movement, which corresponds to the deceleration phase of the squat. Other groups have also investigated muscle activity during the squat, both in healthy and pathological situations [8], and have obtained results similar to ours for their non-pathologic setting.

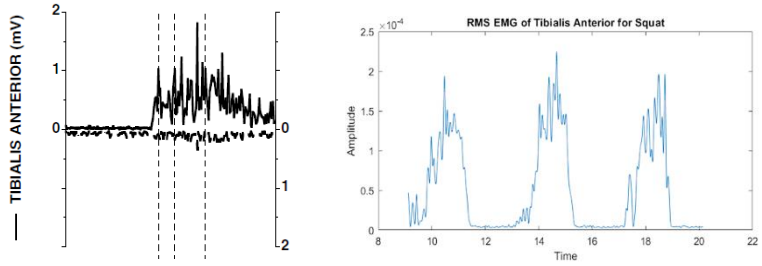

Figure 11: Activation pattern of the Tibialis Anterior during the squat. Left - adapted from the literature [2]; Right - results obtained with our model.

5 Conclusions

In this project, we analyzed the kinematics of gait and squat movement of a healthy subject, using a MATLAB implementation.

For the gait analysis, particular interest was given to the foot's position through time, which provided relevant information regarding the subject's gait cycle, and to the angles of relevant joints (hip, knee, ankle). All parameters seem to be in accordance with what can be found in the literature, indicating the probable lack of abnormalities in the subject's gait. As for the squat movement, the same angle joints were considered, and the results seem to be in accordance with the former conclusions.

Ultimately, our findings indicate that we have built a robust model for the kinematic analysis of biomechanical motion. Our healthy subject displayed adequate kinematic and muscle activation patterns, and the plots obtained from the model itself accurately recreate the performed motion.

6 Other Remarks

Although our model seems to produce results which are coherent with the current literature, it is important to note its limitations. For instance, the model is inherently limited by the motion tracking system that was used for data acquisition, both in regard to number of datapoints (related to the number of markers and to the different acquisition timepoints) and to the relative movement of the markers attached to the skin with respect to the joints. Another limitation of this model is the fact that we are performing a 2-dimensional analysis, which can neglect crucial factors for understanding the motion of the individual.

Another important note is that, while the chosen model type might be useful, it is not necessarily the only valid one. There are a multitude of other modeling techniques which are available, one of which being Self-Organizing Maps (SOMs). SOMs are particular architectures of Artificial Neural Networks which are utilized to track and analyze motion based on machine learning algorithms. Since this technology is still in its developmental stages, the variety of motions that can be analyzed is still rather small. SOMs have already been employed to analyze gait and squat and can therefore be considered an alternative method to the one presented in this work [10]. Other methods of biomechanical analysis are also being explored, such as a marker-free, webcam-dependent image acquisition software, which is capable to detect human motion and depict it in a sufficiently accurate fashion just by making use of an 8MP webcam and image processing algorithms, without the need for any position markers [11]. This particular implementation, although incomplete, is especially relevant in poorer regions, which often lack the resources to conduct a more thorough evaluation and can be expected to be developed in the coming years.

References

[1] Schoenfeld, B. J. (2010, December). Squatting kinematics and kinetics and their application to exercise performance. *Journal of Strength and Conditioning Research*, Vol. 24, pp. 3497–3506. https://doi.org/10.1519/JSC.0b013e3181bac2d7

[2] Whittle, Michael W. *Gait Analysis – An Introduction*. 4th Edition; Elsevier; 2007.

[3] Winter, D. A. (2009). Biomechanics and Motor Control of Human Movement: Fourth Edition. In *Biomechanics and Motor Control of Human Movement: Fourth Edition*. https://doi.org/10.1002/9780470549148

[4] Nikravesh, P. E. (1988). Computer-Aided Analysis of Mechanical Systems. In *Prentice-Hall, Englewood Cliffs, New Jersey* (Vol. 110).

[5] J. Ambrósio, "Kinematics of multibody systems." Week 02, Lecture 05, 2020

[6] D. Winter, *The biomechanics and motor control of human gait*. University of Waterloo Press, 1987.

[7] Schoenfeld, B. J. (2010). Squatting Kinematics and Kinetics and Their Application to Exercise Performance. *Journal of Strength and Conditioning Research*, *24*(12), 3497–3506. https://doi.org/10.1519/JSC.0b013e3181bac2d7

[8] Dionisio, V. C., Almeida, G. L., Duarte, M., & Hirata, R. P. (2008). Kinematic, kinetic and EMG patterns during downward squatting. *Journal of Electromyography and Kinesiology*, *18*(1), 134–143. https://doi.org/10.1016/j.jelekin.2006.07.010

[9] Slater, L. V., & Hart, J. M. (2017). Muscle Activation Patterns During Different Squat Techniques. *Journal of Strength and Conditioning Research*, *31*(3), 667–676. https://doi.org/10.1519/JSC.0000000000001323

[10] Blanco Diaz, C. F., Katerine Quitian González, A., Isaza, S. J., & Orjuela-Cañón, A. D. (2019). A Biomechanical Analysis of Free Squat Exercise Employing Self-Organizing Maps. *2019 IEEE Colombian Conference on Applications in Computational Intelligence, ColCACI 2019 - Proceedings*. https://doi.org/10.1109/ColCACI.2019.8781991

[11] Talle Shridevi, A., & Pardeshi, S. A. (2015). Kinematic study of video gait analysis. *2015 International Conference on Industrial Instrumentation and Control, ICIC 2015*, 1208–1213. https://doi.org/10.1109/IIC.2015.7150931

Appendix A - Anthropomorphic Table

Tab. 1: Anthropometric table, retrieved from J. Ambrósio, "Kinematics of multibody systems." Week 07, Lecture 21, 2020

Segment	Definition	Segment Weight/Total Body Weight	Center of Mass/ Segment Length		Radius of Gyration/ Segment Length		
			Proximal	Distal	C of G	Proximal	Distal
Hand	Wrist axis/knuckle II middle finger	0.006 M	0.506	0.494 P	0.297	0.587	0.577 M
Forearm	Elbow axis/ulnar styloid	0.016 M	0.430	0.570 P	0.303	0.526	0.647 M
Upper arm	Glenohumeral axis/elbow axis	0.028 M	0.436	0.564 P	0.322	0.542	0.645 M
Forearm and hand	Elbow axis/ulnar styloid	0.022 M	0.682	0.318 P	0.468	0.827	0.565 P
Total arm	Glenohumeral joint/ulnar styloid	0.050 M	0.530	0.470 P	0.368	0.645	0.596 P
Foot	Lateral malleolus/head metatarsal II	0.0145 M	0.50	0.50 P	0.475	0.690	0.690 P
Leg	Femoral condyles/medial malleolus	0.0465 M	0.433	0.567 P	0.302	0.528	0.643 M
Thigh	Greater trochanter/femoral condyles	0.100 M	0.433	0.567 P	0.323	0.540	0.653 M
Foot and leg	Femoral condyles/medial malleolus	0.061 M	0.606	0.394 P	0.416	0.735	0.572 P
Total leg	Greater trochanter/medial malleolus	0.161 M	0.447	0.553 P	0.326	0.560	0.650 P
Head and neck	C7–T1 and 1st rib/ear canal	0.081 M	1.000	— PC	0.495	0.116	— PC
Shoulder mass	Sternoclavicular joint/glenohumeral axis	—	0.712	0.288	—	—	—
Thorax	C7–T1/T12–L1 and diaphragm*	0.216 PC	0.82	0.18	—	—	—
Abdomen	T12–L1/L4–L5*	0.139 LC	0.44	0.56	—	—	—
Pelvis	L4–L5/greater trochanter*	0.142 LC	0.105	0.895	—	—	—
Thorax and abdomen	C7–T1/L4–L5*	0.355 LC	0.63	0.37	—	—	—
Abdomen and pelvis	T12–L1/greater trochanter*	0.281 PC	0.27	0.73	—	—	—
Trunk	Greater trochanter/glenohumeral joint*	0.497 M	0.50	0.50	—	—	—
Trunk head neck	Greater trochanter/glenohumeral joint*	0.578 MC	0.66	0.34 P	0.503	0.830	0.607 M
Head, arms, and trunk (HAT)	Greater trochanter/glenohumeral joint*	0.678 MC	0.626	0.374 PC	0.496	0.798	0.621 PC
HAT	Greater trochanter/mid rib	0.678	1.142	—	0.903	1.456	—

Appendix B - Implementation

Tab. 1: Information contained on each struct. Global variables: Data/ Static Data, Body, Jnt and Output. Further explanation for a better code understanding is presented in directly commented on the Matlab script.

Data/Static Data	Body	Jnt	Output

• Frequency
• Coordinates
	• Number
	• PtsAdj
	• COM
	• Pi
	• Pj
	• Length
	• theta
	• Eta
	• r
	• csi
	• A
	• B
		• NRevolute
		• NGround
		• NDriver
		• Revolute
		  ○ i
		  ○ j
		  ○ spPi
		  ○ spPj
		• Driver
		  ○ type
		  ○ i
		  ○ ctype
		  ○ j
		  ○ Data
		  ○ q
		  ○ qd
		  ○ qdd
			• Time
			• Body
			  ○ r
			  ○ theta
			  ○ rd
			  ○ thetad
			  ○ rdd
			  ○ thetadd
			  ○ COM
			  ○ length
			• Revolute
			  ○ i
			  ○ j
			  ○ spPi
			  ○ spPj
			• Driver
			  ○ type
			  ○ i
			  ○ ctype
			  ○ j
			  ○ Data
			  ○ q
			  ○ qd
			  ○ qdd

Appendix C - Kinematic Results of Gait Analysis

C.1 Trunk

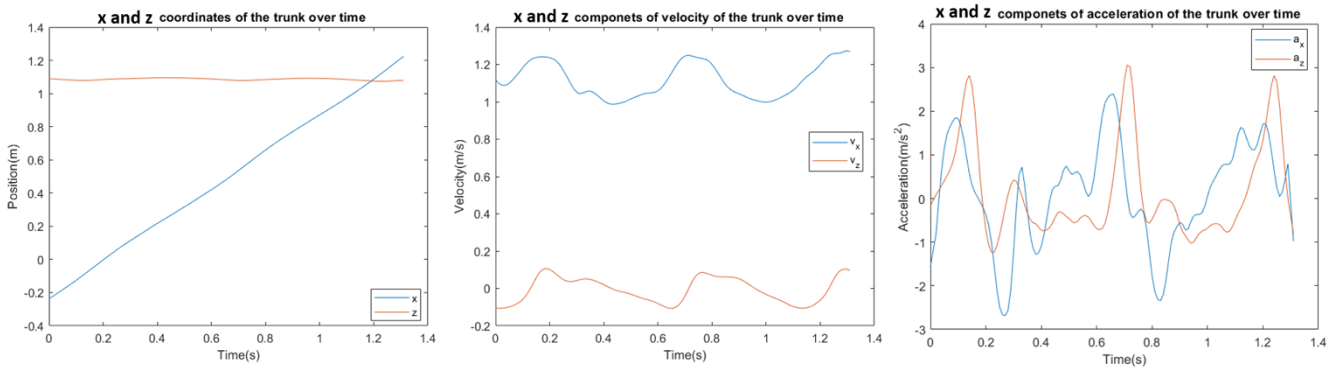

Figure 1: Kinematic results of gait analysis: position, velocity and acceleration of the trunk over time.

C.2 Left Limb

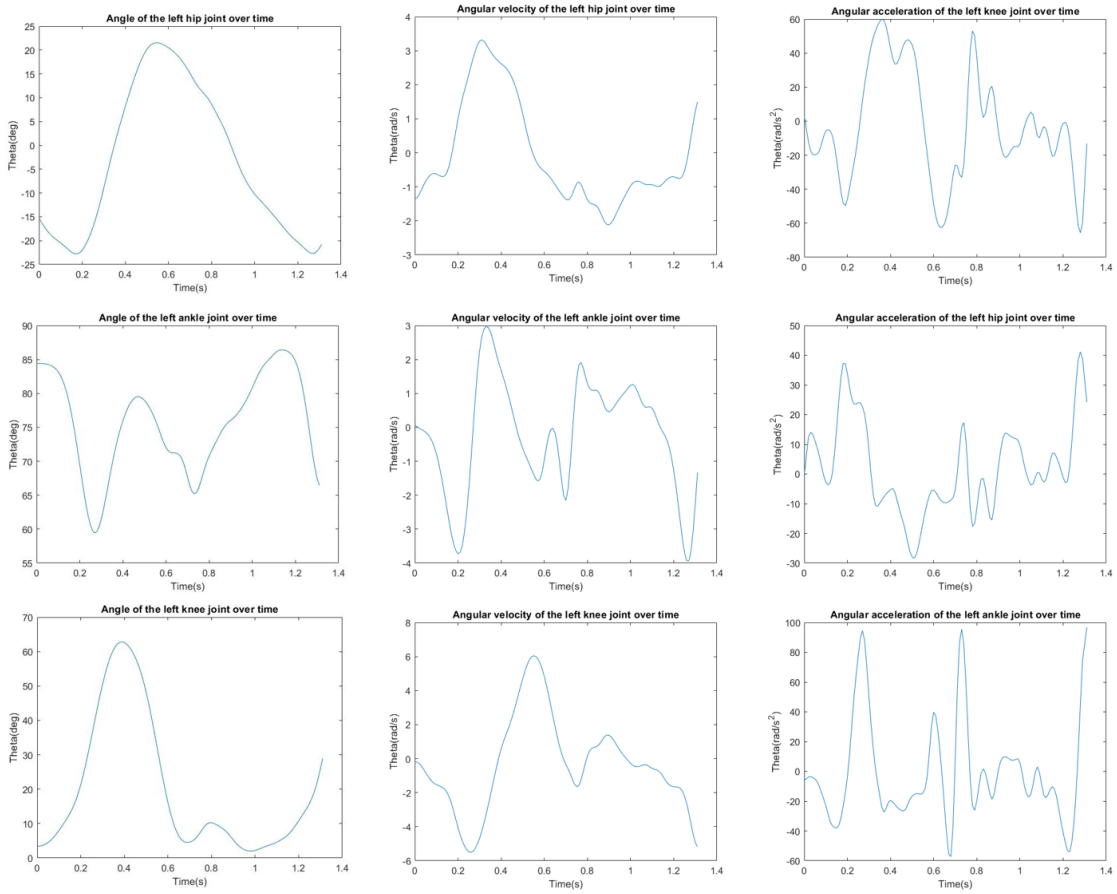

Figure 2: Kinematic results of gait analysis for the left limb: angle, angular velocity and angular acceleration for the hip, left knee and left ankle joints over time.

C.3 Right Limb

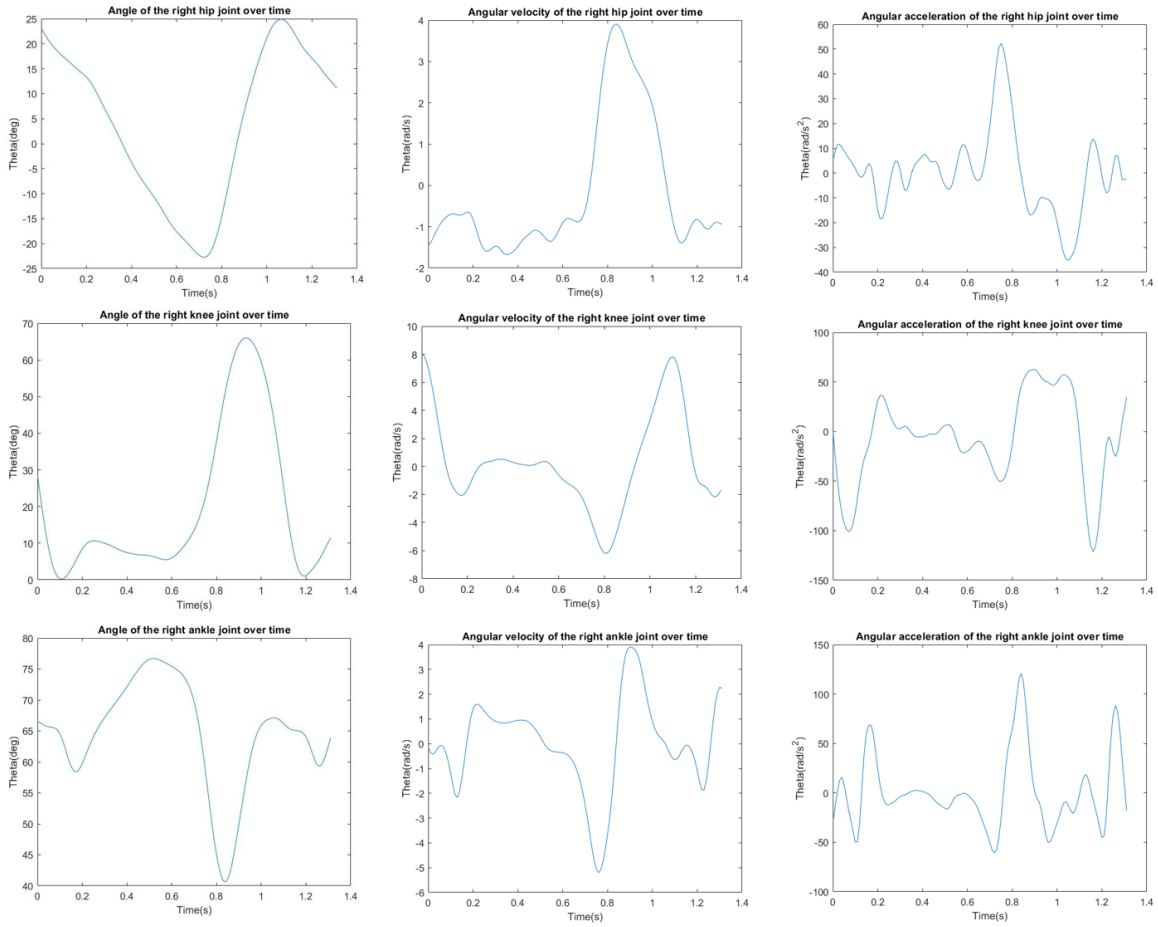

Figure 3: Kinematic results of gait analysis for the right limb: angle, angular velocity and angular acceleration for the hip, left knee and left ankle joints over time.

Appendix D – Literature Kinematic Results for Stride

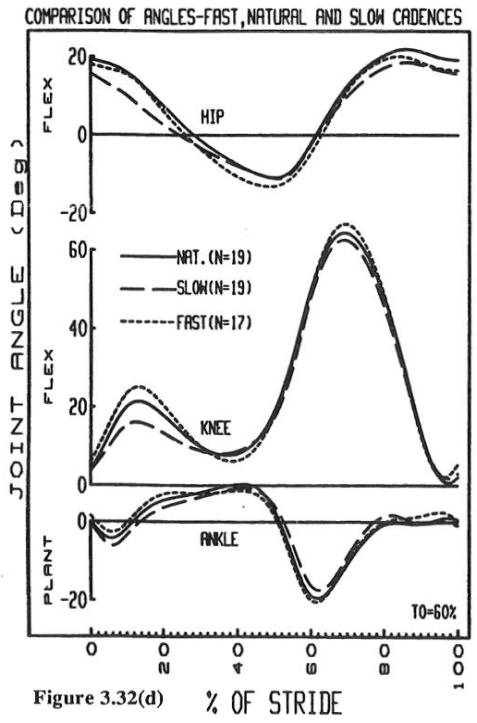

Figure 3.32(d)

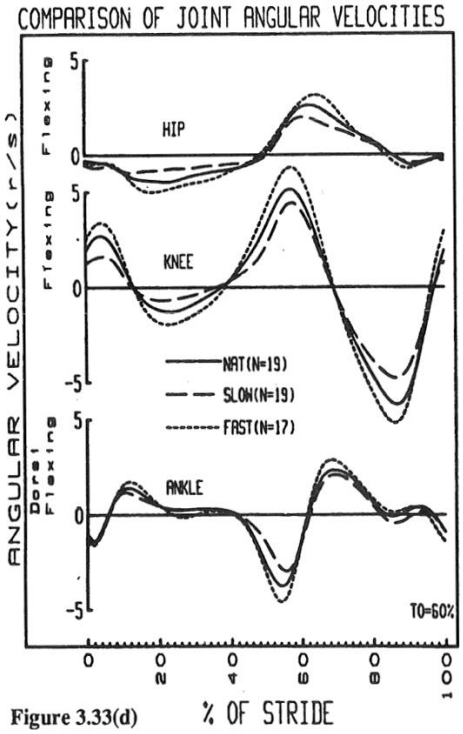

Figure 3.33(d)

(A) (B)

Figure 1: Results from literature for the joint angles and joint angular velocities for the hip, knee and ankle. Retrieved from D. Winter, *The biomechanics and motor control of human gait*. University of Waterloo Press, 1987.

Appendix E - Electromyography (EMG) Results for Gait Analysis

E.1 RM EMG

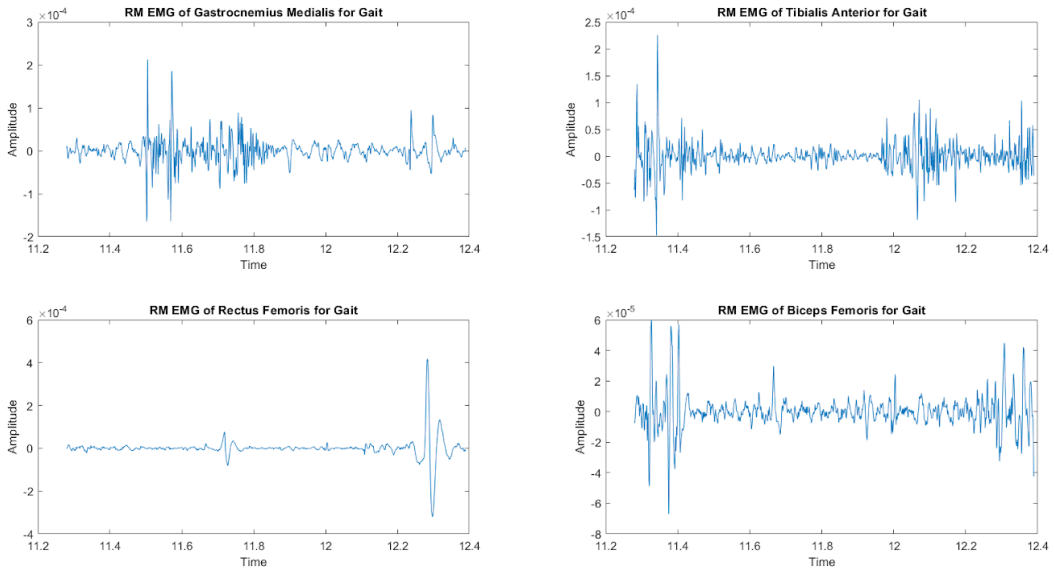

Figure 1: Electromyographic results (EMG) for gait analysis: Amplitude of the Gastrocnemius Medialis, Tibialis Anterior, Rectus Femoris and Biceps Femoris over time.

E.2 Root-Mean-Squared (RMS) EMG

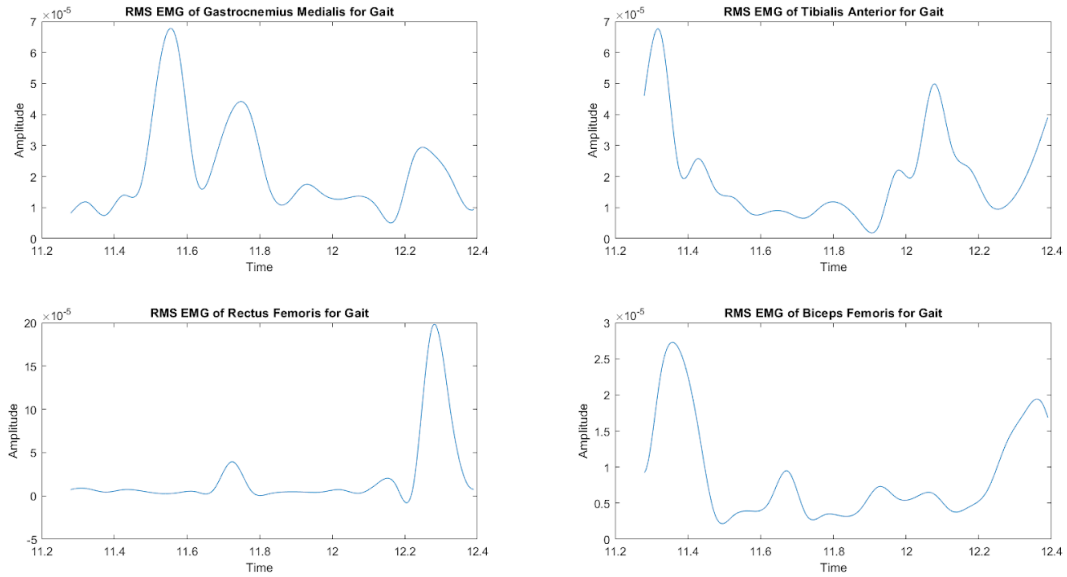

Figure 2: Root-mean squared electromyographic results (EMG) for gait analysis: Amplitude of the Gastrocnemius Medialis, Tibialis Anterior, Rectus Femoris and Biceps Femoris over time.

Appendix F - Kinematic Results of Squat Analysis

F.1 Trunk

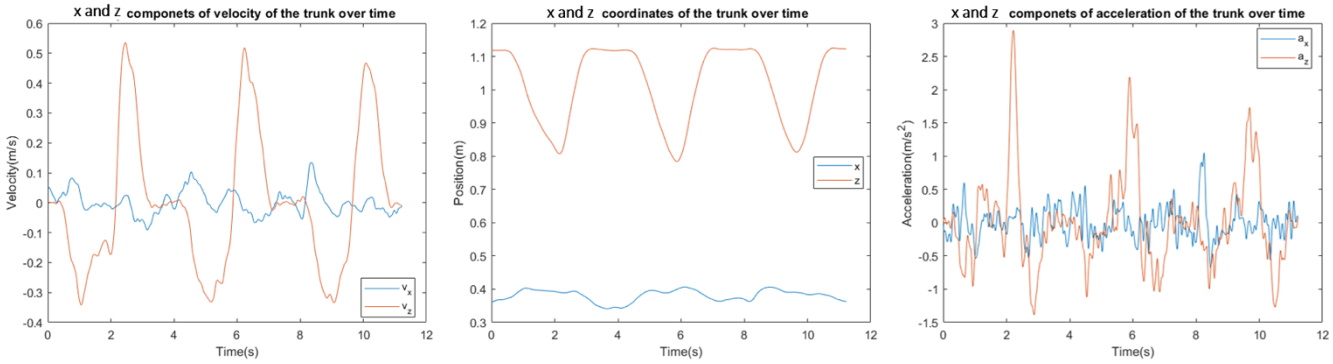

Figure 1: Kinematic results of squat analysis: position, velocity and acceleration of the trunk over time.

F.2 Left Limb

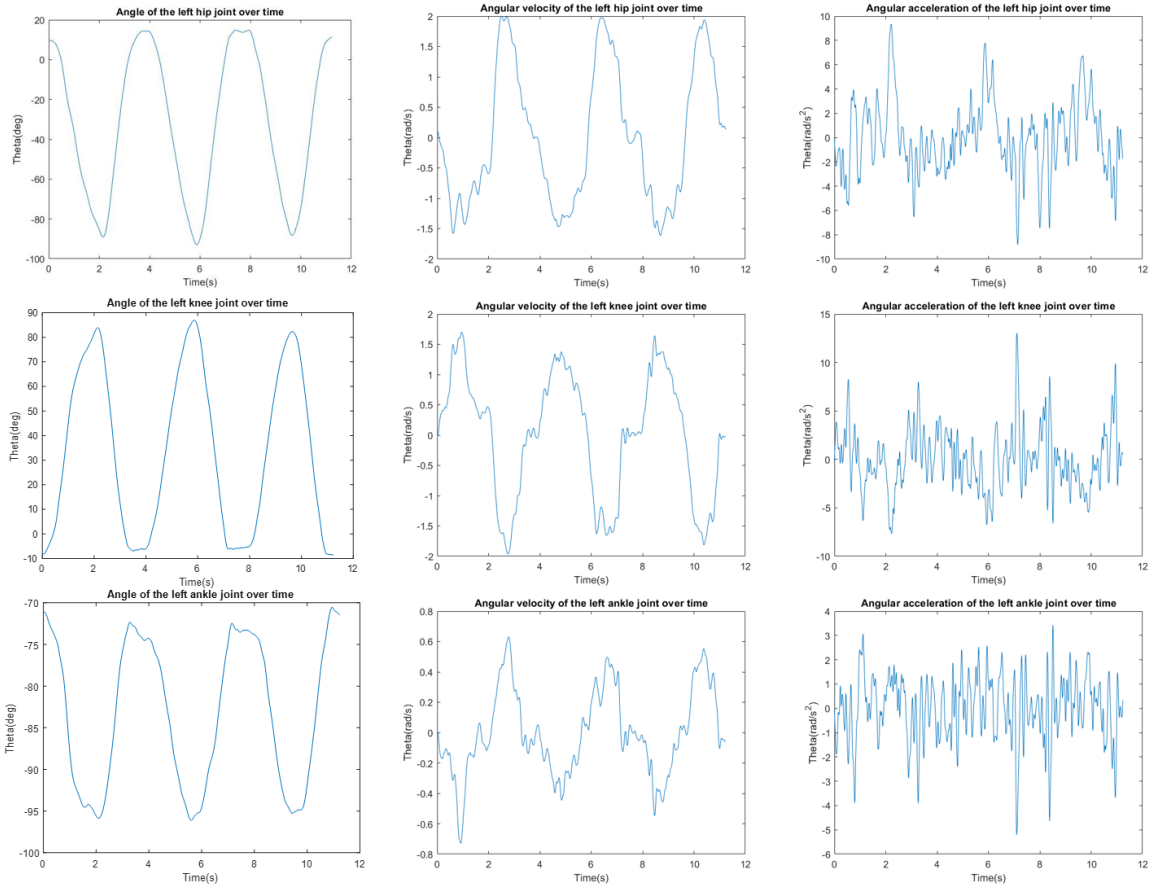

Figure 2: Kinematic results of gait analysis for the left limb: angle, angular velocity and angular acceleration for the hip, left knee and left ankle joints over time.

F.3 Right Limb

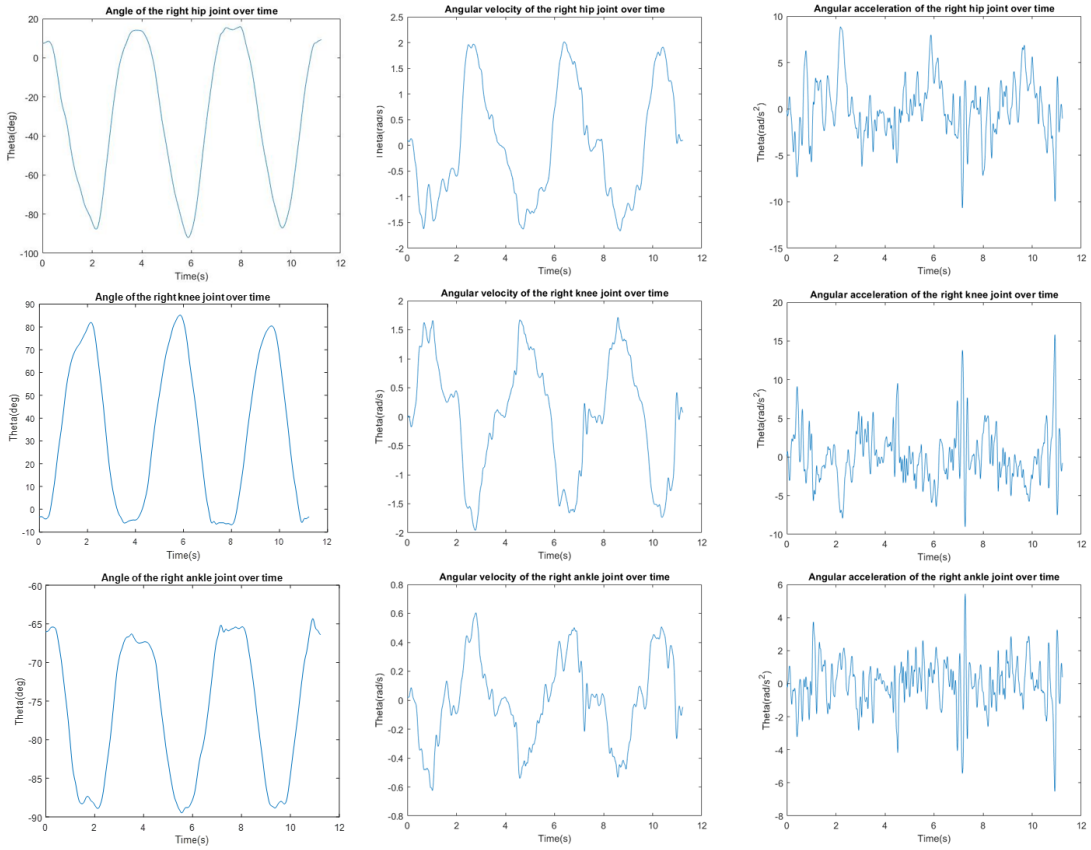

Figure 3: Kinematic results of gait analysis for the right limb: angle, angular velocity and angular acceleration for the hip, left knee and left ankle joints over time.

Appendix G – Literature Kinematic Results for Squat

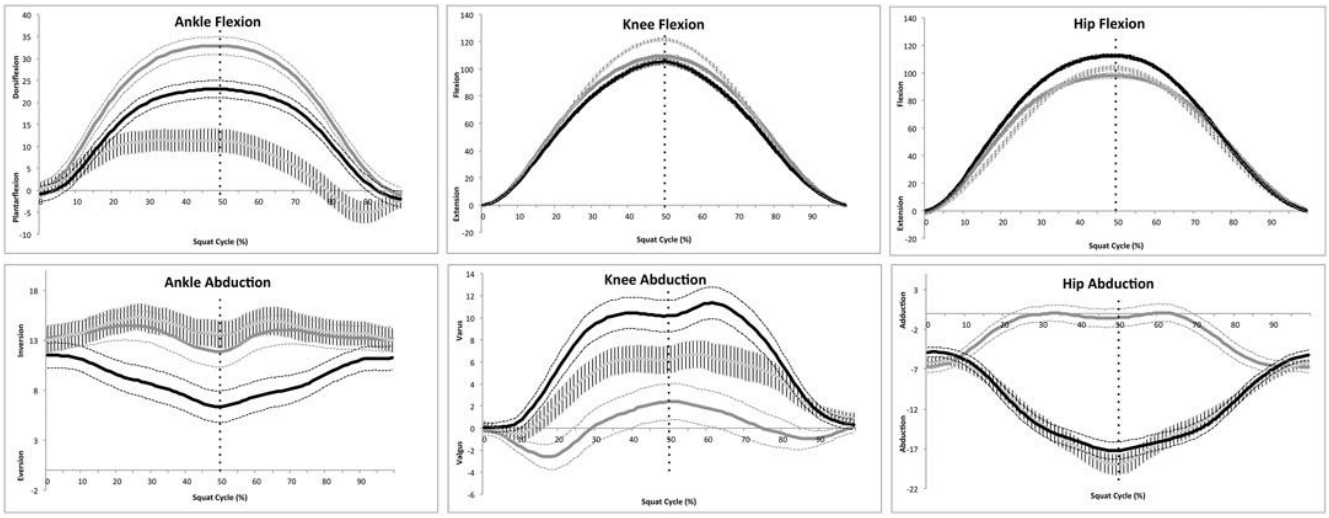

Figure 1: Angles for the hip and knee. Retrived from Slater, L. V., & Hart, J. M. (2017). Muscle Activation Patterns During Different Squat Techniques. *Journal of Strength and Conditioning Research*, *31*(3), 667–676. https://doi.org/10.1519/JSC.0000000000001323

Appendix H - EMG Results for Squat Analysis

H.1 RM EMG

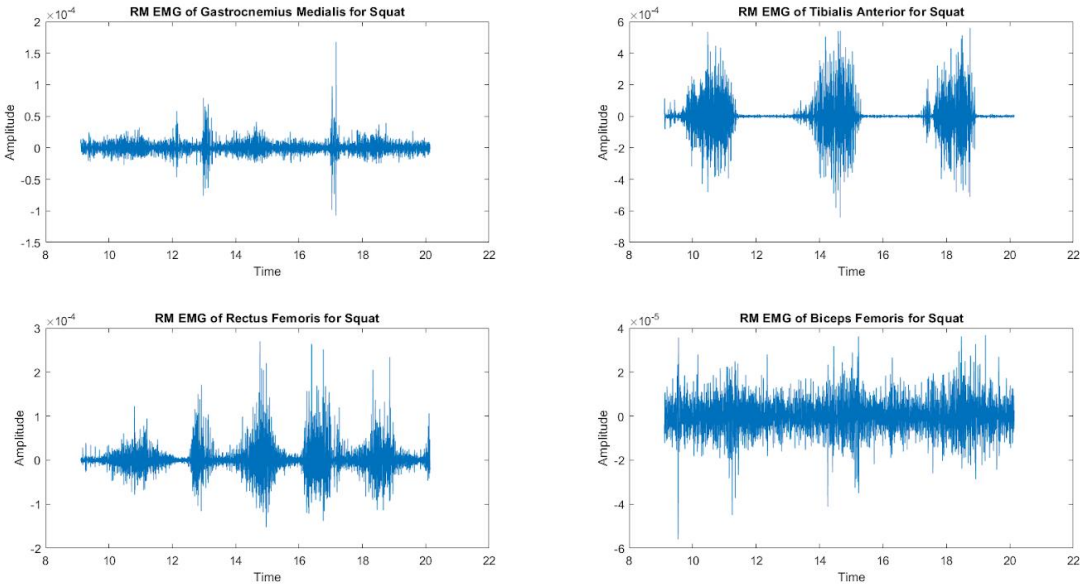

Figure 1: Electromyographic results (EMG) for squat analysis: Amplitude of the Gastrocnemius Medialis, Tibialis Anterior, Rectus Femoris and Biceps Femoris over time.

H.2 RMS EMG

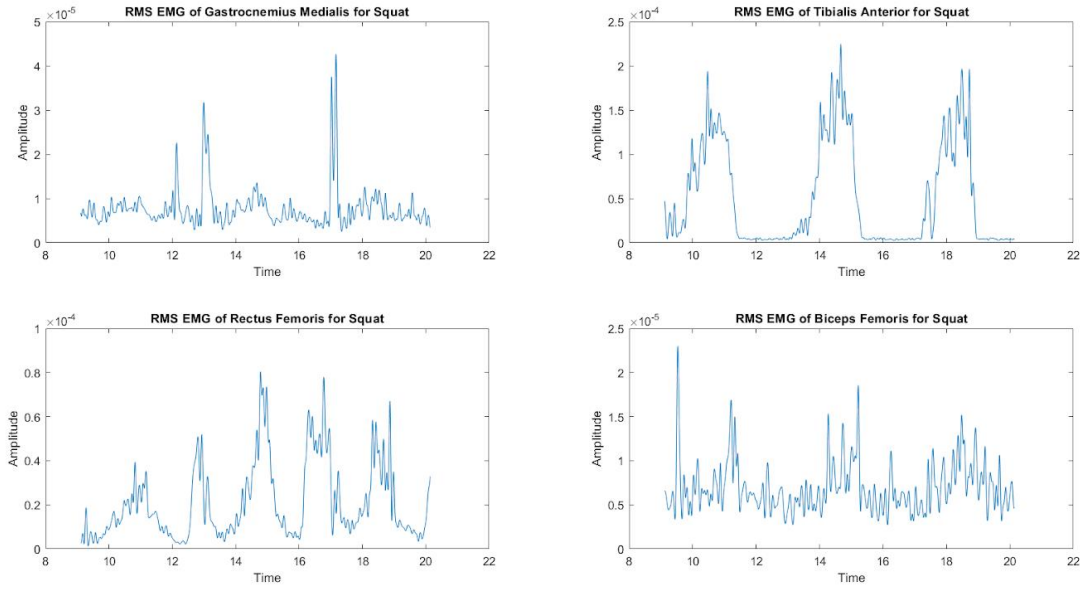

Figure 2: Root-mean squared electromyographic results (EMG) for squat analysis: Amplitude of the Gastrocnemius Medialis, Tibialis Anterior, Rectus Femoris and Biceps Femoris over time.